

CORONAL ALFVÉN SPEED DETERMINATION: CONSISTENCY BETWEEN SEISMOLOGY USING AIA/*SDO* TRANSVERSE LOOP OSCILLATIONS AND MAGNETIC EXTRAPOLATION

E. VERWICHTE^{1,2}, T. VAN DOORSSELAERE², C. FOULLON¹, AND R. S. WHITE¹

¹ Centre for Fusion, Space and Astrophysics, Department of Physics, University of Warwick, Coventry CV4 7AL, UK; Erwin.Verwichte@warwick.ac.uk

² Centre for Plasma Astrophysics, Department of Mathematics, Katholieke Universiteit Leuven, Celestijnenlaan 200B, B-3001 Leuven, Belgium

Received 2012 December 18; accepted 2013 February 8; published 2013 March 20

ABSTRACT

Two transversely oscillating coronal loops are investigated in detail during a flare on the 2011 September 6 using data from the Atmospheric Imaging Assembly (AIA) on board the *Solar Dynamics Observatory*. We compare two independent methods to determine the Alfvén speed inside these loops. Through the period of oscillation and loop length, information about the Alfvén speed inside each loop is deduced seismologically. This is compared with the Alfvén speed profiles deduced from magnetic extrapolation and spectral methods using AIA bandpass. We find that for both loops the two methods are consistent. Also, we find that the average Alfvén speed based on loop travel time is not necessarily a good measure to compare with the seismological result, which explains earlier reported discrepancies. Instead, the effect of density and magnetic stratification on the wave mode has to be taken into account. We discuss the implications of combining seismological, extrapolation, and spectral methods in deducing the physical properties of coronal loops.

Key words: magnetohydrodynamics (MHD) – Sun: corona – Sun: magnetic topology – Sun: oscillations

Online-only material: color figures

1. INTRODUCTION

The solar corona and the structures therein, such as loops, support magnetohydrodynamic (MHD) waves of various kinds (Deforest & Gurman 1998; Aschwanden et al. 1999; Berghmans & Clette 1999; Kliem et al. 2002; Verwichte et al. 2005; Tomczyk et al. 2007). Transverse waves and in particular transverse loop oscillations (TLOs) have received much attention because they are manifestations of waves supported by the magnetic field and plasma structuring of the corona (Aschwanden et al. 1999; Nakariakov et al. 1999; Verwichte et al. 2004; Tomczyk et al. 2007; McIntosh et al. 2011). The synoptic, full-disk nature of Atmospheric Imaging Assembly (AIA) on board *Solar Dynamics Observatory* (*SDO*; Lemen et al. 2012) observations confirms that they are ubiquitous and are present in many eruptive events (White & Verwichte 2012). TLOs occur in loops of all sizes and temperatures, and have periods spanning a few to tens of minutes (e.g., Aschwanden et al. 2002; Verwichte et al. 2010; White & Verwichte 2012; White et al. 2012).

The comparison of the observed wave quantities with MHD wave theory provides a seismological route to determining local physical parameters that are difficult to measure directly (e.g., Verwichte et al. 2006b; Arregui et al. 2006; Goossens et al. 2008). Nakariakov & Ofman (2001) demonstrated that by measuring the period and wavelength of the oscillation an estimate of the loop’s Alfvén speed and local magnetic field strength can be obtained. Knowledge of those physical parameters is important for modeling dynamics in the solar corona such as solar flares and coronal mass ejections. Various authors have reported phase speeds typically of the order of 1000 km s⁻¹. The determination of the Alfvén speed from the observed phase speed lies at the heart of the seismological method and employs the wave theory for kink modes. The basic theory by Edwin & Roberts (1983) applies to internally uniform loops. However, to improve accuracy, effects such as density and magnetic stratification can be incorporated (Andries et al. 2005, 2009). In all versions of the wave theory, knowledge of the density contrast between the

loop and the external corona is required to find the Alfvén speed. However, the exact value of the density contrast is difficult to measure directly (e.g., Aschwanden et al. 2003; Schmelz et al. 2003; Terzo & Reale 2010).

Aschwanden & Schrijver (2011) were the first to compare a seismologically determined magnetic field with a potential magnetic extrapolation. The seismologically determined magnetic field strength had been extracted using the density measured using a DEM method applied to the AIA bandpasses (Aschwanden et al. 2011; Hannah & Kontar 2012). They found that the average extrapolated magnetic field strength in the loop exceeded the seismologically determined value by a factor of three. We wish to establish the physical reasons for such a discrepancy. Because the loop’s magnetic field strength is derived from the Alfvén speed by using the loop density (deduced from spectral measurement or from assumption), the Alfvén speed is the true seismologically determined physical loop quantity. We shall therefore determine the Alfvén speed from a new TLO event using AIA data and compare it with the Alfvén speed obtained by spectral and magnetic extrapolation methods. This has become feasible because of the superior quality of the AIA instrument and the multiple viewpoints made possible by the Extreme UltraViolet Imager (EUVI) on board *STEREO* (Howard et al. 2008; Wuelser et al. 2004; Verwichte et al. 2009).

The paper is organized as follows. In Section 2, we present the wave analysis two TLOs seen by AIA. In Section 3 the Alfvén speed using the “direct” methods of magnetic extrapolation and Differential Emission Measure (DEM) inversion is calculated. In Section 4 the role of stratification is examined in determining the equivalent Alfvén speed to compare with wave observations. In Section 5, the results from the comparison are used to determine the loop cross-section profile. Finally, in Section 6 we discuss our findings and explore its potential and limitations.

2. TRANSVERSE LOOP OSCILLATION EVENT

We examine two loops in NOAA active region 11283 on 2011 September 6, which exhibit transverse oscillations of

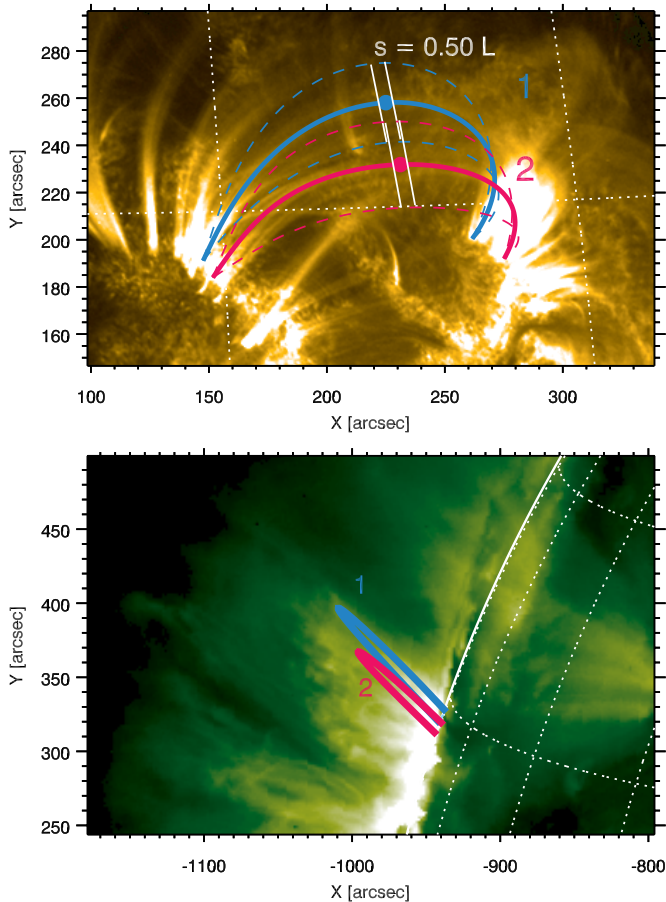


Figure 1. Detailed view of the loops at 22:15:30 UT in AIA/SDO 171 Å (top) and in EUVI/STEREO-A 171 Å (bottom).

(A color version of this figure is available in the online journal.)

periods around 2–3 minutes in response to a GOES class X2.1 flare inside the region starting at 22:12 UT and peaking at 22:20 UT. The location of these loops as seen by AIA/SDO in the 171 Å bandpass is shown in Figure 1. Following the technique detailed in Verwichte et al. (2010) and White & Verwichte (2012), the loops are compared with their view in images from EUVI/STEREO-A 171 Å at 22:15 UT to determine the general 3d geometry (see Figure 1). STEREO-A is ahead of Earth by 103° in longitude. To the projected loop path a third coordinate is added under the assumption that the whole loop lies within a plane. The inclination of that plane with respect to the photospheric normal, θ , is now the only free parameter. The model loop is then transformed to the second viewpoint and θ is adjusted visually to best match the loop seen there. The three-dimensional loop geometry gives loop lengths of 213 Mm and 188 Mm, respectively. The loop geometry parameters are listed in Table 1.

We employ the tried and tested analysis technique for transverse oscillations that has been perfected by several studies (Verwichte et al. 2004, 2009, 2010; Van Doorselaere et al. 2007; White & Verwichte 2012). A rectangular box region of interest (data cut) is chosen that runs across the loop top in the direction aligned with the projected displacement of a hypothetical horizontally polarized TLO. This process is illustrated in Figure 2. The AIA time series are then interpolated at the region of interest locations. For each time, we average the data over the 11 pixel width of the box to increase

Table 1
Physical Loop Quantities

Quantities	Loop #1	Loop #2
Loop geometry		
Loop length L	188 ± 20 Mm	160 ± 20 Mm
Loop inclination angle θ	27° N	25° N
Loop height h	64 Mm	49 Mm
Footpoint separation $\Delta\alpha$	$7:1$	$7:6$
Oscillation parameters		
Oscillation period P	150 ± 5 , s	122 ± 6 , s
Damping time τ	216 ± 60 , s	348 ± 400 , s
Displacement amplitude ξ_0	6.9 ± 1 Mm	1.9 ± 1 Mm
Phase ϕ	$340 \pm 10^\circ$	$299 \pm 30^\circ$
Reference time t_0	22 : 04 UT	22 : 04 UT
Mode number n	1	1
Wavelength λ	380 ± 40 Mm	320 ± 30 Mm
Phase speed V_{ph}	2510 ± 400 km s $^{-1}$	2620 ± 400 km s $^{-1}$
Seis. Alfvén speed $V_{A,s}$	$1780\text{--}2510$ km s $^{-1}$	$1860\text{--}2620$ km s $^{-1}$
Extrapolated quantities		
Av. magn. field $\langle B \rangle$	26 G	41 G
Weig. magn. field $\langle B_W \rangle$	19 G	32 G
Footpoint density $n_{e,fp}$	$0.7 \cdot 10^{15}$ m $^{-3}$	$0.7 \cdot 10^{15}$ m $^{-3}$
Density scaleheight H	65 Mm	139 Mm
Loop temperature T_0	0.79 MK	0.79 MK
Loop minor radius a	0.95 Mm	0.85 Mm
Alfvén speed scaleheight Λ	107 Mm	98 Mm
Loop top Alfvén speed $V_{A,top}$	1470 km s $^{-1}$	1640 km s $^{-1}$
Av. Alfvén speed $\langle V_A \rangle$	2960 km s $^{-1}$	3430 km s $^{-1}$
Weig. Alfvén speed $\langle V_{A,W} \rangle$	2260 km s $^{-1}$	2700 km s $^{-1}$
Dir. Alfvén speed $V_{A,d}$	2130 km s $^{-1}$	2480 km s $^{-1}$
Loop cross-sectional profile		
Inverse density contrast ζ^{-1}	0.4 (0.1–0.9)	0.8 (0.3–1)
Transition layer thickness ℓ/a	1.1 (0.6–2)	1.9 (0–2)

the signal-to-noise ratio. Thus, the data set is reduced to a two-dimensional time-space image set containing the spatial average intensity along the region of interest as a function of time. A TLO would appear as a periodic displacement of the loop location. To obtain the loop axis displacement, we fit a Gaussian shape (Carcedo et al. 2003) superimposed on a linear trend. The width of the fitted Gaussian profile is taken to be a good measure of error on the position. Finally, from the position a trend is subtracted and the loop’s oscillation displacement time series, $\xi(t)$, is obtained, which is characterized by fitting a damped cosine function of the form $\xi(t) = \xi_0 \exp[-(t - t_0)/\tau] \cos[2\pi(t - t_0)/P + \phi]$ using a Levenburg–Marquardt least-squares fitting method Markwardt (2009). The fitting parameters are the displacement amplitude, ξ_0 , oscillation period, P , damping time, τ , phase, ϕ , and reference time, t_0 . The oscillation parameters are listed in Table 1.

The phase speed, V_{ph} , is calculated as the ratio of the wavelength (for fundamental standing mode $\lambda = 2L$) over the period, where we allow for an error of typically 10% in L . For the two loops, we find phase speeds in the range 2500–2600 km s $^{-1}$. By interpreting the TLO as a Alfvénic kink mode in a thin, cylindrical loop uniform in the longitudinal direction and in the zero plasma- β limit, the phase speed is equal to the kink speed, C_K , given by (Edwin & Roberts 1983)

$$C_K \approx \sqrt{\frac{2}{1 + \zeta^{-1}}} V_A, \quad (1)$$

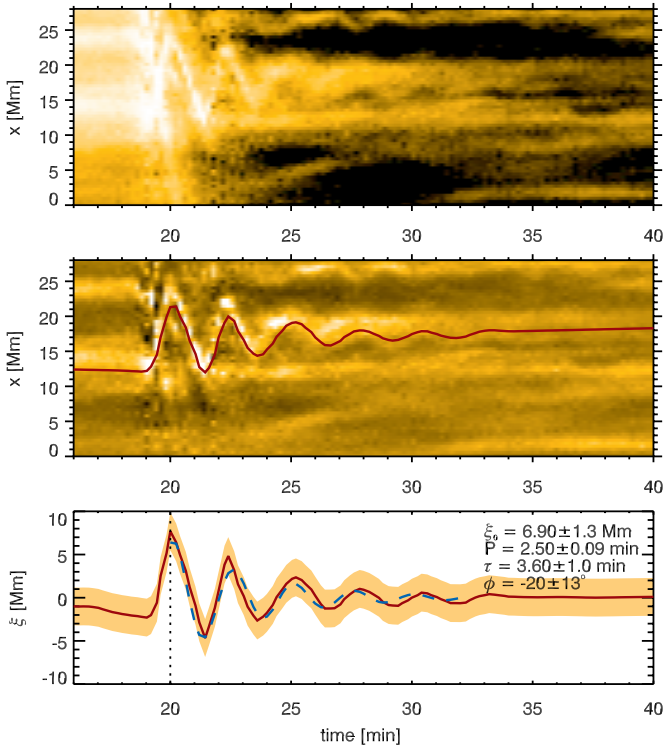


Figure 2. Time–distance image of full intensity for the path at $s = 0.5 L$. Time is counted in minutes from reference time 22:00 UT on 2011 September 6. Middle: filtered time–distance image with the loop position of loop #1 of Event A indicated. Bottom: displacement time series $\xi(t)$. The dashed line is a fitted damped sinusoidal curve. The dotted line indicated the start time used for the fit.

(A color version of this figure is available in the online journal.)

where $\zeta = \rho_{0i}/\rho_{0e}$ is the ratio of internal to external densities and V_A is the Alfvén speed in the loop. We can thus calculate from the phase speed the value range of the loop Alfvén speed,

$$V_{A,s} = V_{ph} \sqrt{\frac{1 + \zeta^{-1}}{2}}, \quad (2)$$

considering the two extreme values of ζ , namely unity and infinity for an overdense loop. The exact value of the density contrast is difficult to measure (e.g., Aschwanden et al. 2003; Schmelz et al. 2003; Terzo & Reale 2010). Expression (2) assumes that the loop is uniform with the internal Alfvén speed equal to $V_{A,s}$ all along the loop. However, it is expected that the loops are stratified in density and magnetic field strength and that the Alfvén speed varies along the loop. Aschwanden & Schrijver (2011) equate $V_{A,s}$ with the average speed in the loop for to the same travel time.

3. COMPARISON BETWEEN SEISMOLOGICAL AND DIRECT DETERMINATION OF ALFVÉN SPEED

The Alfvén speed $V_{A,s}$ can be exploited seismologically to determine the loop magnetic field strength (Nakariakov & Ofman 2001). However, in order to do so the value of the loop density is required. Often in the absence of spectroscopic information of the loop density, and employing the argument that the density appears only weakly (through a square root) in the Alfvén speed, a plausible value of the electron number density $n_e = 10^{15} \text{ m}^{-3}$ had been assumed (Verwichte et al. 2004). For this density, we find values for the magnetic field strength for

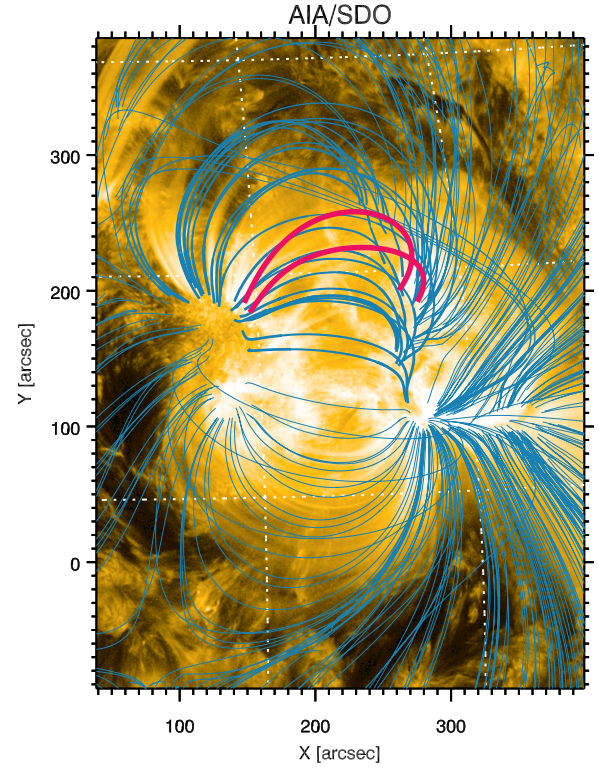


Figure 3. PFSS potential-field extrapolation of active region NOAA 11283 on 2011 September 7 at 00:00 UT. The two oscillating loops are indicated in red. (A color version of this figure is available in the online journal.)

each loop in the ranges 25–46 G and 25–48 G, respectively. If we assume a density one order of magnitude smaller, we find values of 8–15 G for both loops instead. We shall attempt to test the consistency of the seismological method by estimating the magnetic field and loop density independently. We can then compare the average Alfvén speeds from both methods.

First, the magnetic field is determined using the Potential Field Source Surface (PFSS) potential-field extrapolation tool (Schrijver 2001; Schrijver & De Rosa 2003), which produces a data cube of all three components of magnetic field in spherical coordinates. Figure 3 shows the potential-field extrapolation of the active region. The projected loop paths are indicated in red. The magnetic field is interpolated for the three-dimensional loop paths. We can see that the paths approximately align with the potential field, but not fully. Misalignments with an angle between 20° and 40° between potential-field extrapolations and loops have been reported in the past (Sandman et al. 2009). The average ratio of parallel to total magnetic field strength is 60%. Importantly, for our study only the field strength is required, which is expected to be less sensitive. The top panels in Figures 4 and 5 show the magnetic field strength along the loop.

We estimate the density of the loops from the AIA bandpasses following a method outlined in Aschwanden & Schrijver (2011). However, as the loops are only seen clearly in the 171 Å bandpass, we assume that the temperature of the loop corresponds to the peak temperature of that bandpass. The observed intensity, normalized with exposure time, is related to the differential emission measure as

$$I_{171} = \int_0^{\infty} \text{DEM}(T) R_{171}(T) dT, \quad (3)$$

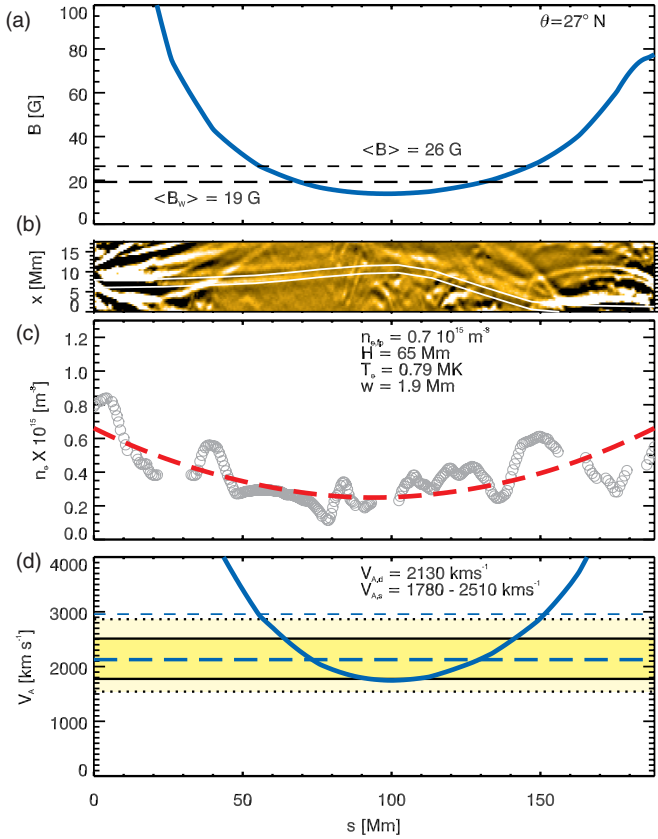


Figure 4. For loop #1, a comparison of the Alfvén speed derived seismologically and derived using magnetic extrapolation with potential fields and spectroscopy using *SDO/AIA* bandpasses. (a) Magnetic field strength from PFSS model at 2011 September 7 (00:00 UT), interpolated along the 3d path of the loop. The magnetic field averages (B) and (B_w) are indicated as dashed and long-dashed lines, respectively. (b) AIA 171 Å intensity along the path of the loop. The detailed location of the loop is indicated by two solid lines. (c) Electron number density derived using Equation (5) as a function of distance along the loop. The dashed line is a fit of the form (6). (d) Alfvén speed as a function of distance along the loop. The thick blue curve is the Alfvén speed along the loop determined using Equation (7). The horizontal shaded region is the range of values for the seismologically determined Alfvén speed, $V_{A,s}$, using Equation (2) for an arbitrary value of the loop density contrast. The light shaded region bordered by dotted lines extends this range by including the measurement errors of loop length and oscillation period. The thin dashed line is the average Alfvén speed (V_A). The thick blue dashed line is the Alfvén speed, $V_{A,d}$.

(A color version of this figure is available in the online journal.)

where $R_{171}(T)$ is the response function for the 171 Å bandpass. The contribution to the intensity from the loop itself is determined from fitting at each position along the loop a Gaussian profile with background. Assuming an isothermal plasma, the DEM becomes trivially

$$\text{DEM}(T) = n_e^2 \text{LOS} \delta(T - T_0), \quad (4)$$

where n_e is the electron number density, $\text{LOS}(s)$ is the distance across the loop, which takes into account the geometry of the loop with respect to the line-of-sight direction, and $T_0 = 0.79$ MK is the peak temperature of the 171 Å bandpass. Then, the loop electron number density is found as

$$n_e(s) = \sqrt{\frac{I_{\text{loop}}(s)}{R_{171}(T_0) \text{LOS}(s)}}. \quad (5)$$

Because we assume that the temperature corresponds to the peak temperature of the bandpass (i.e., $R_{171}(T_0)$ is maximal), the thus

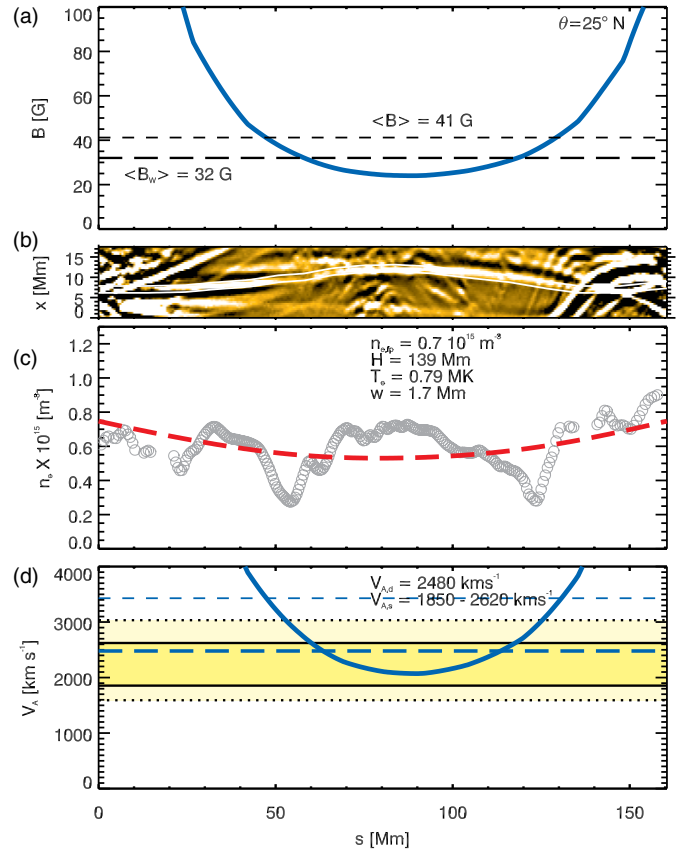


Figure 5. Same as Figure 4 but for loop #2.

(A color version of this figure is available in the online journal.)

determined that density may be regarded as a lower limit. Panels (c) of Figures 4 and 5 show the density as a function of distance along the loop. We find the density to vary between 10^{14} and 10^{15} m^{-3} . The profile is noisy due to line-of-sight interference but a clear trend of decreasing density toward the loop top can be seen. We fit an exponential function to the density profile of the form

$$n_e(s) = n_{e,\text{fp}} e^{-\frac{z(s)}{H}}, \quad (6)$$

where z is the height above the photosphere and H is the density scale height. We find values for the density scale height of 65 Mm and 139 Mm, respectively. If we assume an isothermal loop, these would correspond to temperatures of 1.3 MK and 2.8 MK, respectively. The loops probably do not have these temperatures as they are not clearly visible in the 193 Å and 211 Å bandpasses, whose peak temperature is in this range. So-called super-hydrostatic density scale heights have been determined before (e.g., Van Doorselaere et al. 2007).

In panels (d) we combine the magnetic field strength and electron density and find the Alfvén speed as a function of distance along the loop as

$$V_A(s) = \frac{B(s)}{\sqrt{\mu_0 \tilde{\mu} m_p n_e(s)}}, \quad (7)$$

where $\tilde{\mu} = 1.2$ for coronal abundances. The average Alfvén speed across the loop, (V_A), is defined as the constant speed that gives the same travel time between the two foot points

(Aschwanden & Schrijver 2011):

$$\int_0^L \frac{ds}{V_A(s)} = \Delta t = \frac{L}{\langle V_A \rangle} \Rightarrow \langle V_A \rangle = L \left[\int_0^L \frac{ds}{V_A(s)} \right]^{-1}. \quad (8)$$

Figures 4 and 5 show that the average Alfvén speed exceeds the seismologically determined Alfvén speed range by up to a factor of two. This result is consistent with what was found by Aschwanden & Schrijver (2011). It seems to indicate that there is a mismatch between seismological and direct methods in determining the loop Alfvén speed. Following the definition of the average Alfvén speed, we calculate the average magnetic field as

$$\langle B \rangle = L \left[\int_0^L \frac{ds}{B(s)} \right]^{-1}, \quad (9)$$

where $B(s)$ is the magnetic field strength along the three-dimensional loop path. For the two loops, we find that the magnetic field strength varies between more than 100 G at the foot points to values around or below 20 G at the loop tops. The average magnetic field strength is 26 G and 41 G, respectively. These values fall within the range that was found seismologically with $n_e \sim 10^{15} \text{ m}^{-3}$.

We may improve the averaging by including a weight that takes into account the localization of wave energy along the loop. Thus, the average Alfvén speed is modified to be

$$\langle V_{A,W} \rangle = L \left[\int_0^L \frac{W(s) ds}{V_A(s)} \right]^{-1}, \quad (10)$$

with weight function

$$W(s) = n_e(s) \xi^2(s) L \left[\int_0^L n_e(s) \xi^2(s) ds \right]^{-1}. \quad (11)$$

Here $\xi(s)$ is the mode displacement profile. When not using the mode profile from solving Equation (12), it may be approximated using $\xi(s) = \xi_0 \sin(\pi s/L)$. The average magnetic field may be weighted in the same manner. As Table 1 shows, the weighted average Alfvén speeds for the two loops lie closer to the seismological Alfvén speed range but is still represents an overestimation.

4. ROLE OF STRATIFICATION

We wish to take the analysis a step further and consider the role of stratification on the TLO. The longitudinal structuring of the Alfvén speed will modify the oscillation period and phase speed (Andries et al. 2009). In the thin flux-tube limit, the spatial structure of a TLO may be modeled using the following differential equation (Dymova & Ruderman 2005, 2006; Verth & Erdélyi 2008):

$$\frac{d^2 \eta(s)}{ds^2} + \frac{\omega^2}{C_K^2(s)} \eta(s) = 0, \quad (12)$$

where $\eta(s) = \xi/a$ is the transverse loop displacement relative to the local loop radius and ω is the mode frequency. Instead of modeling the kink speed in Equation (12) using a range of values of ζ , we take an alternate approach. We introduce $\tilde{\omega} =$

$\sqrt{1 + \zeta^{-1}} \omega / \sqrt{2}$. We assume that ζ is constant along the loop. Then Equation (12) is modified to

$$\frac{d^2 \eta}{ds^2} + \frac{\tilde{\omega}^2}{V_{A,d}^2(s)} \eta = 0. \quad (13)$$

From the resulting modified mode frequency, we define a phase speed, $V_{A,d}$, as

$$V_{A,d} = \frac{\tilde{\omega} L}{\pi}. \quad (14)$$

We have two approaches to solve Equation (13). In the first approach, we solve Equation (13) completely numerically using a Runge–Kutta algorithm with adaptive step size (Press et al. 2007). The mode frequency $\tilde{\omega}$ is then found using a shooting method. A second approach is to first solve Equation (13) analytically by modeling the Alfvén speed profile with an exponential profile of the form $V_A(s) = V_{A,\text{top}} \exp(|s - L/2|/\Lambda)$ where Λ represents a typical scale height of the Alfvén speed. Then, the solution of Equation (13) with zero foot point displacement is in terms of Bessel functions of order 0 (Ferraro & Plumpton 1958; McEwan et al. 2008)

$$\eta(s) = \eta_0 [Y_0(kx_L)J_0(kx) - J_0(kx_L)Y_0(kx)], \quad (15)$$

where $k = \tilde{\omega} \Lambda / V_{A,\text{top}} = (\Lambda \pi / L)(V_{A,d} / V_{A,\text{top}})$, $x_L = \exp(-L/2\Lambda)$ and $x = \exp(-|s - L/2|/\Lambda)$. The wave frequency $\tilde{\omega}$, and through Equation (14) also $V_{A,d}$, is then found as the fundamental mode solution of the dispersion relation

$$Y_0(kx_L)J_1(k) - J_0(kx_L)Y_1(k) = 0, \quad (16)$$

which is solved numerically using, e.g., a bracketing root-finding algorithm. For the two loops using the Alfvén speed profiles from Figures 4 and 5 we find fit values of $\Lambda = 107 \text{ Mm}$ and 98 Mm , and $V_{A,\text{top}} = 1470 \text{ km s}^{-1}$ and 1640 km s^{-1} , respectively. The numerically derived values are listed in Table 1.

We have determined $V_{A,d}$ using both numerical and analytical approaches and they give equivalent results. Figures 4 and 5 show that for both loops $V_{A,d}$ (found with the numerical approach) falls inside the observed range of Alfvén speeds. This suggests that the seismological and direct methods are consistent.

It also shows the importance of interpreting correctly the observed Alfvén speed range. Our findings indicate that the average Alfvén speed $\langle V_A \rangle$ is not necessarily a good measure to compare with the seismology. Figure 6 shows the dependency of $\tilde{\omega}$ on Λ and this may be used to quickly read the solution for given Λ without need of explicitly solving Equation (13). The solution is fitted by a power law of the form

$$V_{A,d} = V_{A,\text{top}} \left[1 + 0.27 \left(\frac{\Lambda}{L} \right)^{-0.93} \right]. \quad (17)$$

Figure 6 also clearly illustrates the disparity between the full solution and the use of the average Alfvén speed, which becomes significant for $\Lambda \lesssim L$. In the case studies, $\Lambda/L \approx 0.5$ and $\langle V_A \rangle$ is nearly 1.5 times as large as $V_{A,d}$.

5. DETERMINATION OF THE LOOP CROSS-SECTIONAL PROFILE

If we equate the Alfvén speed $V_{A,s}$ in Equation (2) with $V_{A,d}$, then we can directly calculate the density contrast ζ , i.e.,

$$\zeta^{-1} = 2 \left(\frac{V_{A,d}}{V_{\text{ph}}} \right)^2 - 1, \quad (18)$$

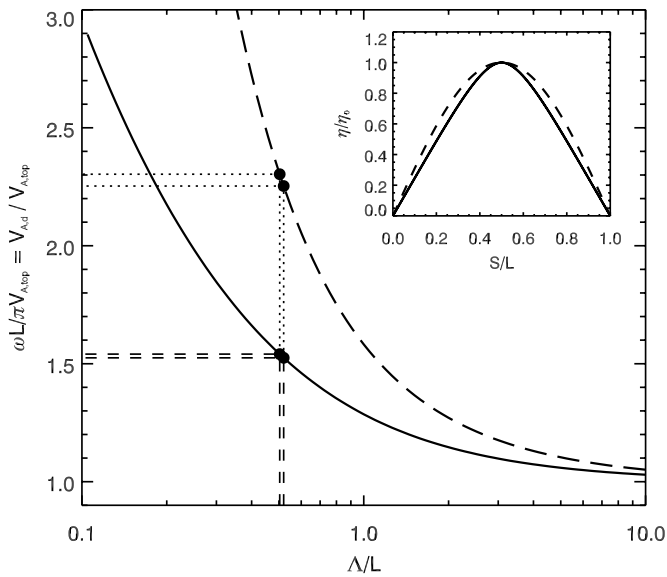


Figure 6. Normalized Alfvén speed $V_{A,d}/V_{A,top} = \tilde{\omega}L/\pi V_{A,top}$ as a function of normalized Alfvén speed scale height Δ/L from solving Equation (13). The long-dashed curve corresponds to the solution using the average Alfvén speed $\langle V_A \rangle$. The values corresponding to the two loops are indicated. The inset shows the displacement profile along the loop. The dashed line is a sine curve.

assuming ζ is constant along the loop. For loops #1 and #2 we find values of $\zeta^{-1} = 0.4$ and $\zeta^{-1} = 0.8$, respectively. Note that the uncertainties are large. We may obtain seismologically more information about the loop cross-section by including the observed damping rate. The leading theory that explains the rapid damping of the oscillations is resonant absorption. It critically depends on the thickness of a thin transition layer, ℓ , over which the density drops from inner to external conditions. Under the assumption of small thickness, $\ell \ll a$, it is given by (e.g., Ionson 1978; Hollweg & Yang 1988; Goossens et al. 1992; Ruderman & Roberts 2002)

$$\frac{\ell}{a} = F \frac{\zeta + 1}{\zeta - 1} \frac{P}{\tau}, \quad (19)$$

where ℓ/a is between 0 and 2. For a half-wavelength sinusoidally varying density profile across the layer, $F = 2/\pi$ (Ruderman & Roberts 2002). Equation (19) is strictly speaking only in the regime where $\ell \ll a$, though it still provides a relatively accurate extension into the regime of finite resonance layer widths (Van Doorselaere et al. 2004). Also, Equation (19) does not describe any transient behavior in the damping (Pascoe et al. 2012). From the previous sections we have estimates of all parameters in Equation (19), except for ℓ/a . We can thus determine its value. We find $\ell/a = 1.1$ for loop #1 and $\ell/a = 1.9$ for loop #2. The uncertainties are large and cover the whole [0,2] interval for loop #2. The uncertainty on ℓ/a for loop #2 is large due to the large uncertainty in the damping time.

6. DISCUSSION

We have determined the Alfvén speed in a coronal loop using two independent methods: a seismological method applied to a TLO and a direct method taking the effects of density and magnetic stratification into account and based on magnetic potential-field extrapolation and spectral information from the AIA bandpasses. We have repeated the study for two oscillating loops seen by AIA/SDO during the same flaring event, using

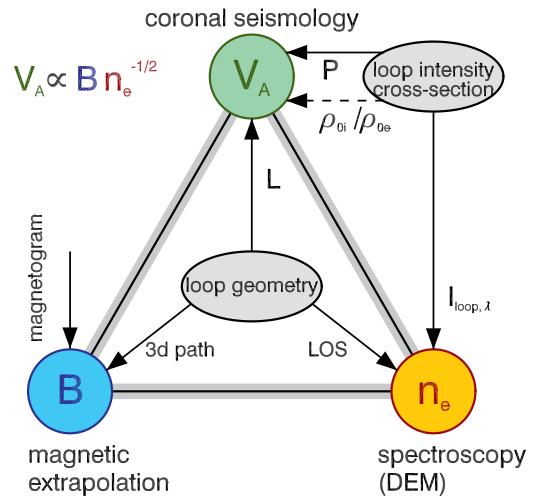


Figure 7. Principle how the techniques of coronal seismology, magnetic extrapolation, and spectroscopy and their determination of the Alfvén speed, magnetic field strength, and density are linked with each other through the formula of the Alfvén speed.

(A color version of this figure is available in the online journal.)

the 171 Å bandpass. For both loops, both methods give consistent results, which demonstrates that the technique of coronal seismology produces valid results. We have demonstrated that it is important to correctly interpret the observed Alfvén speed range from the oscillations. It is not sufficient to compare with an average Alfvén speed along the loop, which explains the discrepancy that Aschwanden & Schrijver (2011) initially found.

In turn, when using a seismologically determined value of the Alfvén speed, $V_{A,s}$, as input for modeling or for comparison with other types of observational data, it is important to understand what this value means with respect to the Alfvén speed profile of the loop. Equation (17), where $V_{A,d}$ is replaced by $V_{A,s}$, provides a method for connecting the measurement with the Alfvén speed profile along a longitudinally stratified loop as represented by a loop top value and a scale height.

A main conclusion to draw from this study is that seismological techniques should not be seen in isolation from other methods. We have shown that through the formula of the Alfvén speed, the techniques of coronal seismology, magnetic extrapolation, and spectroscopy are linked. Figure 7 illustrates the connections graphically. Thus, combining information from multiple techniques allows to construct more advanced methods of determining physical loop parameters or/and to build in consistency checks. We can envisage several scenarios. The obvious first scenario is the determination of the loop’s magnetic field (assuming a longitudinally uniform loop) where the density from spectroscopy is combined with the Alfvén speed from seismology (Nakariakov & Ofman 2001). When including the effect of stratification at least two parameters are required to model the Alfvén speed profile. To resolve these parameters purely seismologically, it requires a detailed measurement of the spatial wave displacement profile or of multiple wave harmonics (Andries et al. 2009). However, when this is not available, magnetic extrapolation and spectroscopy can provide alternate information. We have provided a figure (Figure 6) to help find without calculation the expected Alfvén speed $V_{A,d}$ from the Alfvén speed at the loop top and the Alfvén speed scale height. Lastly, as demonstrated in Section 5, when combining all

methods we can obtain information about the density contrast and transition layer thickness, which were impossible to determine separately by purely seismological means (Arregui et al. 2008; Goossens et al. 2008).

We have also looked at applying the same comparison between seismological and direct methods of determining the Alfvén speed to off-limb events but encountered the difficulty of obtaining an accurate value of the density due to large line-of-sight confusion. Also, the three-dimensional path is less precise in that case because it is established using EUVI/STEREO as the reference (instead of the other way round for on-disk events seen by AIA/SDO). Furthermore, the magnetic extrapolation is inaccurate as it is constructed from older or later magnetogram data from near the limb.

We add the following caveats to this study. First, the magnetic extrapolation is based on a potential-field model that has limitations for active regions, where it is expected that free magnetic energy is stored in the field, which ultimately drives eruptions (Wiegmann & Sakurai 2012). Alignment between the visible loop and the magnetic field can be improved by employing force-free extrapolation models (e.g., Régnier et al. 2008) instead and using magnetic maps from HMI/SDO. Second, the determination of the density relied on the observation from the 171 Å bandpass alone. Therefore, the determined density is only a lower limit. Ideally, we wish to obtain a better constraint on the density by using multiple bandpasses (Aschwanden et al. 2011; Hannah & Kontar 2012) and may also incorporate density measurements from at least one loop location using spectrometer data (from, e.g., EIS/Hinode; Culhane et al. 2007). Third, it is critical for the three-dimensional geometry of the loop to be determined accurately. We have repeated the analysis for different loop inclination angles. A change of 5° causes $V_{A,d}$, derived from extrapolation, to vary between the bottom and top range of the seismologically determined Alfvén speed range. Therefore, the derived values of loop contrast ζ and transition layer thickness ℓ , which already have large uncertainties attached, have to be interpreted with caution.

Finally, we have not included the effect of curvature or structuring in the external corona (e.g., non-constant ζ along the loop) that may give rise to lateral wave leakage (Brady & Arber 2005; Verwichte et al. 2006a; Van Doorselaere et al. 2009; Pascoe et al. 2009), which modifies the relation between observed phase and kink speed as well as contributes to the observed oscillation damping. For thin coronal loops this effect is expected to be secondary.

E.V. acknowledges financial support from the UK Science and Technology Facilities Council (STFC) on the CFSA Rolling Grant and the SF fellowship SF/12/004 of the KU Leuven Research Council. T.V.D. acknowledges funding from the Odysseus programme of the FWO-Vlaanderen and the EU's Framework Programme 7 as ERG 276808. C.F. acknowledges financial support from STFC under her Advanced Fellowship ST/I003649/1. R.S.W. acknowledges support of an STFC Ph.D. studentship. AIA data are courtesy of SDO (NASA) and the AIA consortium. We thank the SOHO, STEREO, and SDO instrument teams for making data available used in this paper, and Dr. Marc de Rosa for useful discussions about the PFSS package.

REFERENCES

- Andries, J., Van Doorselaere, T., Roberts, B., et al. 2009, *SSRv*, **149**, 3
- Arregui, I., Ballester, J. L., & Goossens, M. 2008, *ApJL*, **676**, L77
- Arregui, I., Andries, J., Van Doorselaere, T., Goossens, M., & Poedts, S. 2006, *A&A*, **463**, 333
- Aschwanden, M. J., Boerner, P., Schrijver, C. J., & Malanushenko, A. 2011, *SoPh*, **384**, 102
- Aschwanden, M. J., de Pontieu, B., Schrijver, C. J., & Title, A. M. 2002, *SoPh*, **206**, 99
- Aschwanden, M. J., Fletcher, L., Schrijver, C. J., & Alexander, D. 1999, *ApJ*, **520**, 880
- Aschwanden, M. J., Nightingale, R. W., Andries, J., Goossens, M., & Van Doorselaere, T. 2003, *ApJ*, **598**, L375
- Aschwanden, M. J., & Schrijver, C. J. 2011, *ApJ*, **736**, 102
- Berghmans, D., & Clette, F. 1999, *SoPh*, **186**, 207
- Brady, C. S., & Arber, T. D. 2005, *A&A*, **438**, 733
- Carcedo, L., Brown, D. S., Hood, A. W., Neukirch, T., & Wiegmann, T. 2003, *SoPh*, **218**, 29
- Culhane, J. L., Harra, L. K., James, A. M., et al. 2007, *SoPh*, **243**, 19
- Deforest, C. E., & Gurman, J. B. 1998, *ApJL*, **501**, L217
- Dymova, M. V., & Ruderman, M. S. 2005, *SoPh*, **229**, 79
- Dymova, M. V., & Ruderman, M. S. 2006, *A&A*, **457**, 1059
- Edwin, P. M., & Roberts, B. 1983, *SoPh*, **88**, 179
- Ferraro, C. A., & Plumpton, C. 1958, *ApJ*, **127**, 459
- Goossens, M., Arregui, I., Ballester, J. L., & Wang, T. J. 2008, *A&A*, **484**, 851
- Goossens, M., Hollweg, J. V., & Sakurai, T. 1992, *SoPh*, **138**, 233
- Hannah, I. G., & Kontar, E. P. 2012, *A&A*, **539**, A146
- Hollweg, J. V., & Yang, G. 1988, *JGR*, **93**, 5423
- Howard, R. A., Moses, J. D., Vourlidas, A., et al. 2008, *SSRv*, **136**, 67
- Ionson, J. A. 1978, *ApJ*, **226**, 650
- Kliem, B., Dammach, I. E., Curdt, W., & Wilhelm, K. 2002, *ApJL*, **568**, L61
- Lemen, J. R., Title, A. M., Akin, D. J., et al. 2012, *SoPh*, **275**, 17
- Markwardt, C. B. 2009, in ASP Conf. Ser. 411, *Astronomical Data Analysis Software and Systems XVIII*, ed. D. A. Bohlender, D. Durand, & P. Dowler (San Francisco, CA: ASP), 251
- McEwan, M. P., Díaz, A. J., & Roberts, B. 2008, *A&A*, **481**, 819
- McIntosh, S. W., de Pontieu, B., Carlsson, M., et al. 2011, *Natur*, **475**, 477
- Nakariakov, V. M., & Ofman, L. 2001, *A&A*, **372**, L53
- Nakariakov, V. M., Ofman, L., Deluca, E. E., Roberts, B., & Davila, J. M. 1999, *Sci*, **285**, 862
- Pascoe, D. J., de Moortel, I., & McLaughlin, J. A. 2009, *A&A*, **505**, 319
- Pascoe, D. J., Hood, A. W., de Moortel, I., & Wright, A. N. 2012, *A&A*, **539**, A37
- Press, W. H., Teukolsky, S. A., Vetterling, W. T., & Flannery, B. P. 2007, *Numerical Recipes: The Art of Scientific Computing* (Cambridge: Cambridge Univ. Press)
- Régnier, S., Priest, E. R., & Hood, A. W. 2008, *A&A*, **491**, 297
- Ruderman, M. S., & Roberts, B. 2002, *ApJ*, **577**, 475
- Sandman, A. W., Aschwanden, M. J., Derosa, M. L., Wülser, J. P., & Alexander, D. 2009, *SoPh*, **259**, 1
- Schmelz, J. T., Beene, J. E., Nasraoui, K., et al. 2003, *ApJ*, **599**, 604
- Schrijver, C. J. 2001, *ApJ*, **547**, 475
- Schrijver, C. J., & De Rosa, M. L. 2003, *SoPh*, **212**, 165
- Terzo, S., & Reale, F. 2010, *A&A*, **515**, A7
- Tomczyk, S., McIntosh, S. W., Keil, S. L., et al. 2007, *Sci*, **317**, 1192
- Van Doorselaere, T., Andries, J., & Poedts, S. 2007, *A&A*, **471**, 311
- Van Doorselaere, T., Andries, J., Poedts, S., & Goossens, M. 2004, *ApJ*, **606**, 1223
- Van Doorselaere, T., Verwichte, E., & Terradas, J. 2009, *SSRv*, **149**, 299
- Verth, G., & Erdélyi, R. 2008, *A&A*, **486**, 1015
- Verwichte, E., Aschwanden, M. J., Van Doorselaere, T., Foullon, C., & Nakariakov, V. M. 2009, *ApJ*, **698**, 397
- Verwichte, E., Foullon, C., & Nakariakov, V. M. 2006a, *A&A*, **449**, 769
- Verwichte, E., Foullon, C., & Nakariakov, V. M. 2006b, *A&A*, **452**, 615
- Verwichte, E., Foullon, C., & Van Doorselaere, T. 2010, *ApJ*, **717**, 458
- Verwichte, E., Nakariakov, V. M., & Cooper, F. C. 2005, *A&A*, **430**, L65
- Verwichte, E., Nakariakov, V. M., Ofman, L., & Deluca, E. E. 2004, *SoPh*, **223**, 77
- White, R. S., & Verwichte, E. 2012, *A&A*, **537**, A49
- White, R. S., Verwichte, E., & Foullon, C. 2012, *A&A*, **545**, A129
- Wiegmann, T., & Sakurai, T. 2012, *LRSP*, **9**, 5
- Wuelser, J.-P., Lemen, J. R., Tarbell, T. D., et al. 2004, *Proc. SPIE*, **5171**, 111